Effect of covalent and non-covalent linking of zinc(II) phthalocyanine functionalised carbon nanomaterials on the sensor response to ammonia

POLYAKOV, Maxim S., BASOVA, Tamara V., GÖKSEL, Meltem, ŞENOCAK, Ahmet, DEMIRBAŞ, Erhan, DURMUS, Mahmut, KADEM, Burak and HASSAN, Aseel <http://orcid.org/0000-0002-7891-8087>

Effect of covalent and non-covalent linking of zinc(II) phthalocyanine functionalised carbon nanomaterials on the sensor response to ammonia

Maxim S. Polyakov[1], Tamara V. Basova[1,2,*], Meltem Göksel[3,4], Ahmet Şenocak[3], Erhan Demirbaş[3], Mahmut Durmuş[3,*], Burak Kadem[5], Aseel Hassan[5]

[1]*Nikolaev Institutes of Inorganic Chemistry SB RAS, Lavrentiev Pr. 3, Novosibirsk 630090, Russia*

[2]*Novosibirsk State University, Pirogova Str. 2, Russia*

[3]*Gebze Technical University, Department of Chemistry, Gebze, Kocaeli 41400, Turkey*

[4]*Kocaeli University, Kosekoy Vocational School, Department of Chemistry Technology, Kartepe, Kocaeli 41135, Turkey*

[5]*Material and Engineering Research Institute, Sheffield Hallam University, Sheffield, UK*

* Author for correspondence:

Dr. Mahmut Durmuş, Department of Chemistry, Gebze Technical University, Gebze 41400, Kocaeli, Turkey

Tel: 00 90 262 6053019

Fax: 00 90 262 6053105

E-mail: durmus@gtu.edu.tr

Abstract

In this work, a comparative study of the sensor response of single walled carbon nanotubes (SWCNTs) and reduced graphene oxide (rGO) covalently and non-covalently functionalised with1-[N-(2-ethoxyethyl)-4-pentynamide]-8(11),15(18),22(25)-tris-{2-[2-(2-ethoxyethoxy) ethoxy]-1-[2-((2-ethoxy ethoxy)-ethoxy)methyl]ethyloxy}zinc(II) phthalocyanine (ZnPc) to ammonia is carried out. It was shown that in the case of SWCNT-based materials both covalent and non-covalent functionalization with zinc(II) phthalocyanine leads to the increase of the sensor response toward NH_3, while functionalization of reduced graphene oxide causes a decrease in the response. At the same time both covalent and non-covalent linking of zinc(II) phthalocyanine leads to twofold decrease of the sensor recovery times. The sensor response of the carbon nanomaterial (single walled carbon nanotubes or reduced graphene oxide) hybrids covalently functionalised with zinc(II) phthalocyanine is several times higher than in the case of non-covalent linking of zinc(II) phthalocyanine to these nanomaterials, which is in good correlation with the number of zinc(II) phthalocyanine molecules adsorbed onto the SWCNT and rGO walls.

Keywords: Carbon nanomaterials; Phthalocyanine; Covalent functionalization; non- covalent functionalization; Ammonia sensor.

1. Introduction

Carbon materials such as carbon nanotube, graphene, graphene oxide or reduced graphene oxide (rGO) are widely investigated as promising materials for chemical sensing applications [1, 2]. This is mainly due to the large surface to volume ratio in these materials, which can provide significant adsorption sites of various gaseous as well as chemical analytes. Furthermore, the most of carbon nanomaterials exhibit comparatively high conductivity in addition to their high mechanical stiffness and chemical stability.

Defect sites and different oxygen contained groups could enhance adsorption of gases onto the carbon materials surface and make them viable candidates as active materials in chemical detection. For instance, rGO contains such functional groups as epoxide, alcohol and carboxylic acid which do not repair upon hydrazine reduction. This makes rGO a material that has both high electrical conductivity and chemically active defect sites, making it a promising candidate for gas detection. The sensitivity of rGO to some gases, such as NO [1, 2], NO_2, NH_3 [3], Cl_2 [4, 5], H_2 [6], and volatile organic compounds [5, 7] is revealed in several published articles and reviews [8, 9]. Carbon nanotubes (CNT) have also been investigated as chemical sensors toward gases and vapors such as NH_3, NO_2 [10], H_2, CH_4, CO, SO_2, H_2S, H_2O_2 and O_2 [11, 12]. However, the selectivity of chemical sensors based on rGO and CNT usually is not good enough. One of the ways to improve their selectivity is controlled functionalization of the surface of carbon nanomaterials with different molecules in order to define the chemically active cites. The other challenges of the development of rGO- or SWCNT-based hybrid materials are the poor solubility, non-uniform film surface and as a consequence non-reproduced sensor response of non-modified carbon nanomaterials.

Carbon nanomaterials (SWCNT and graphene) are favorable for functionalization with different classes of molecules as well as nanoparticles of metals [13], metal oxides [14, 15] and polymers [16, 17]. For instance, rGO modified by SnO_2 nanoparticles has been investigated for improved detection of NO_2 gas [18]. rGO/SnO_2 hybrid demonstrates a higher sensor response

toward NO_2 than the pristine rGO, providing twice as good synergetic effect between graphene and nanoparticles. Quantum effects dominate the sensing mechanism of metal oxide/carbon nanomaterial sensors; and the nature of metal oxide and the manner of preparation of the composite material make it more selective to one or another analyte [19-21, 22, 23].

Another route for graphene and CNT modification is preparation of composites with polymers and organic molecules [17]. A double-layer consisted of rGO and polyethylenimine (PEI) has been exhibited better sensor response toward CO_2 and shorter recovery time than the pristine rGO and rGO/PEI mixed layers. It has already been shown elsewhere [24-26] that functionalisation with metal phthalocyanines (MPc) may improve the solubility and sensor properties of these carbon materials. Actually, phthalocyanines are known to exhibit high electron charge transfer due to their π-conjugated system [27]. On the other hand, the phthalocyanine derivatives are organic semiconductors that have been applied as chemiresistive sensors [28, 29]. The extended π-electronic system of CNTs and graphene makes them very attractive for manipulating charge transfer by combining with such electrophiles as porphyrins and phthalocyanines [30]. A wide variety of functional groups in MPc molecule is used to attach them either covalently or non-covalently to the surface of rGO [31-33] and CNTs [34-38] to obtain hybrid materials with improved sensor performance. The enhanced sensing properties are attributed to the synergistic effect of MPc and carbon materials in the hybrids due to the strong electron transfer interaction, superior electrical conductivity and gas adsorption activity [36].

In our previous works [39-41], we have directed our research to study the influence of phthalocyanines containing different central metals, symmetric or asymmetric substitution, and type of substitutes on the structural and sensor properties of SWCNT/MPc hybrids. We compared [40] the structural features and sensor properties of SWCNT hybrids with symmetrically octa-polyoxyethylene substituted zinc(II) phthalocyanine and its asymmetrically substituted derivative containing three polyoxyethylene groups and one pyrene group as substituents. It was shown that the interaction of asymmetric zinc(II) phthalocyanine containing

one pyrene substituent with SWCNTs is more favorable than in the case of symmetric without pyrene counterpart that provided a higher sensor response toward ammonia vapor. The influence of central metal in the phthalocyanine molecule on sensor response was also verified [41, 42].

The originality of this work is perceived in providing a comparison in the sensor response of SWCNTs and rGO covalently and non-covalently functionalised with 1-[N-(2-ethoxyethyl)-4-pentynamide]-8(11),15(18),22(25)-tris-{2-[2-(2-ethoxyethoxy)ethoxy]-1-[2-((2-ethoxyethoxy)-ethoxy)methyl] ethyloxy}zinc(II) phthalocyanine, abbreviated as ZnPc, (Fig. 1) toward ammonia. The preparation of the SWCNTs and rGO hybrid materials was described according to the procedure given in our previous work [43]. The effect of covalent and non-covalent linking of the phthalocyanine both to SWCNT and to rGO on the electrical sensor response toward low concentration of ammonia (10-50 ppm) is demonstrated. The selectivity of the films is also examined by measuring changes in the resistance of the sensing layers in the presence of some interfering analytes such as carbon dioxide, ethanol, toluene, dichlorobenzene and chloroform.

2. Experimental details

2.1.Materials and equipments

SWCNT was purchased from Sigma Aldrich. Reduced graphene oxide was obtained from Hazerfen KMETSTAŞ – Zerre Chemistry and Materials Company, Turkey and it was used as a graphene nanomaterial. Reduced graphene oxide used as a graphene nanomaterial was obtained from Hazerfen KMETSTAŞ – Zerre Chemistry and Materials Company, Turkey. The surface area of rGO estimated from BET (Brunauer–Emmett–Teller) (Quantachrome Instruments) was 565 m^2/g; the ratio of C:O measured by SEM-EDX (Scanning electron microscopy with energy dispersive X-ray spectroscopy, Philips XL 30 SFEG) was 4.77. The number of layers determined from AFM (Atomic Force Microscope, Digital Instruments) and TEM (Transmission Electron Microscopy, Tecnai G2 F20 S-TWIN) was in the range from 4 to 7 sheets and the lateral size of rGO flakes was approximately 5 µm.

Preparation of covalently bonded ZnPc-SWCNTs and ZnPc-rGO hybrids was carried out as follows. ZnPc dissolved in DMF was sonicated for 15 min at room temperature. Meanwhile, SWCNT–N3 (or rGO–N3) suspended in DMF was sonicated for 30 min at room temperature. ZnPc solution was then added to the SWCNT–N3 (or rGO–N3) suspension dropwise until completion of the reaction. To this suspension, 1.0 mol% copper(II) sulphate pentahydrate and 5.0 mol% sodium L-ascorbate were added as catalysts at room temperature and the resulting mixture was kept in the microwave oven at 60^{o}C for 2 hours. The non-covalently bonded ZnPc-SWCNTs and ZnPc-rGO hybrids were prepared by sonication of the mixture of SWCNT–N3 (or rGO–N3) suspension and ZnPc solution at room temperature without any catalysis. The synthesis and characterization of hybrids of SWCNTs and rGO covalently and non-covalently functionalised with ZnPc is reported in Ref. [43] in more details.

Thermo-gravimetric analyses (TGA) were carried out using a Mettler Toledo STAR^{e} Thermal Analysis System at a rate of 10^{o}C min^{-1} in nitrogen flow of 50 mL min^{-1}.

2.2. Deposition and characterization of thin films

Thin films of the hybrids were deposited by spin coating of their suspensions in dichloromethane onto glass substrates and on platinum interdigitated electrodes deposited onto glass substrates. The morphologies of the synthesized hybrids were determined by FEI-Nova scanning electron microscopy (SEM) with low magnification (160,000X) and high voltage (10kV).

The average thickness of the deposited films of the investigated hybrids, estimated by spectral ellipsometry (Woolam *M-2000V*^{TM} rotating analyser spectroscopic ellipsometer) was about 150 nm. The spectra of the two ellipsometric parameters Ψ and Δ, representing, respectively, the amplitude ratio $tg(\Psi) = A_p/A_s$ and phase shift $\Delta = \varphi_p - \varphi_s$ between p- and s-components of polarised light, were recorded with the M2000V instrument in the 350–1000nm spectral range using the rotating analyzer principle. Optical parameters of the reflection system,

i.e. thicknesses, refractive indices and extinction coefficients of the substrate and deposited layers, can be obtained by solving the reverse ellipsometric problem numerically:

$$tg(\Psi)\exp(i\Delta) = {R_p}/{R_s} \qquad (1)$$

where R_p and R_s are Fresnel reflection coefficients for p- and s-components of polarized light related to the parameters of reflection system, particularly the thickness (*d*) and refractive index (*n*) of the adsorbed layers, via Fresnel equations [44]. The fitting was performed by solving Fresnel equations many times for different values of *n* and *d* and subsequently minimizing the error function of the experimental and theoretical (calculated) values of Ψ and Δ using one of least-square techniques. Commercial WVASE32® software was provided by J.A. Woollam Co., Inc. for this task. Theoretical fitting to experimental Ψ and Δ spectra was carried out by applying a 2-layer model consisting of organic layer and BK7 glass. The refractive indices of the films of SWCNTs covalently and non-covalently functionalised with ZnPc were 1.48 and 1.42, respectively, while the refractive indices of the films of rGO covalently and non-covalently functionalised with ZnPc were 1.75 and 1.79, respectively.

2.3. Study of sensor properties

The sensing performance of the films was studied against ammonia in the concentration range 10-50 ppm, diluted with high purity argon. Pure commercial ammonia gas was used as an analyte source. The diluted NH_3 was passed through the chamber at a flow rate of 300 mL/min. The films were deposited onto platinum interdigitated Pt electrodes (DropSens, G-IDEPT10) to test their conductivity changes upon interaction with the gaseous ammonia. The dimension of gaps was 10 μm; the number of digits was 125 x 2 with a digit length equal to 6760 μm; cell constant was 0.0118 cm^{-1}. The electrical resistance of the films was measured with Keithley 236 by applying a constant dc voltage of 10 V.

3. Results and Discussion

3.1. Characterization of the hybrid materials

The non-covalently functionalised ZnPc:SWCNTs or ZnPc:rGO materials are prepared by mixing SWCNTs or rGO with the ZnPc using an ultrasonic bath, while SWCNTs and rGO hybrids covalently functionalised with ZnPc moieties are prepared by the reaction of azido substituted SWCNTs or rGO with ZnPc *via* "Click" reaction. The detailed description of the preparation method of the hybrids is given in Ref. [43]. In the case of non-covalently functionalized carbon nanomaterials ZnPc molecules adsorb onto the surface of SWCNTs and rGO due to π-π interaction. The formation of the hybrids was confirmed by UV-Vis absorption, FT-IR and Raman spectroscopy in our previous publication [43]. In the covalently functionalized carbon nanomaterials ZnPc molecules are attached to the surface of SWCNTs and rGO via triazole rings (Fig. 1), forming during "Click" chemistry reaction as confirmed by FT-IR spectroscopy [43].

The morphology of the hybrid films was investigated by scanning electron microscopy (SEM). SEM images of the hybrid films deposited by spin coating are presented in Fig. 2. ZnPc:SWCNT hybrids demonstrate different surface morphology depending on the type of ZnPc bonding. The SWCNT-based hybrids non-covalently functionalised with ZnPc (ZnPc:SWCNTs-non-co) clearly exhibit nanotube features on the surface, while covalently functionalised hybrids (ZnPc:SWCNTs-co) demonstrate a tendency to the formation of bigger aggregates. The surface of the films of rGO-based hybrids is different due to the 2D nature of graphene nanomaterials. The rGO-based hybrid non-covalently functionalised with ZnPc (ZnPc:rGO-non-co) exhibits flakes-like features, while the rGO-based hybrid covalently functionalised with ZnPc (ZnPc:rGO-co) has a tendency to form stacks-like structure.

Thermogravimetric analysis (TGA) is used to estimate the amount of ZnPc molecules non-covalently and covalently anchored on the surface of the carbon nanomaterials (Fig. 3). The TGA data shows a loss of weight about 4.32% for pristine SWCNTs, 10.52% for SWCNT-N_3, 42.96% for ZnPc:SWCNT-co, 33.16% for ZnPc:SWCNT-non-co and 76.80% for ZnPc at

700 °C. The loss of weight observed for pristine SWCNTs between 200 °C and 700 °C may be due to the destruction of the residual amorphous carbon still presented in the nanotubes as well as due to the decarboxylation of the oxidized species. The weight percentages of functional groups on SWCNTs also calculated from the weight loss difference between SWCNTs-N_3 – SWCNTs, ZnPc:SWCNT-co – SWCNT-N_3 and ZnPc:SWCNT-non-co – SWCNT-N_3 are 6.20 32.44 and 22.64, respectively. The number of the azide groups or ZnPc molecules on the carbon nanomaterials were calculated as described in the literature [40]. The number of azide functional groups in SWCNT-N_3 is estimated as 1 per 50 carbon atoms. The amount of ZnPc molecules covalently anchored on the surface of the nanotubes as a real ratio is 42.24% (32.44%/76.80%). It is estimated that the per 192 carbon atoms on ZnPc:SWCNT-co contains one ZnPc molecule according to the calculation of ((57.76%x1684.423)/(42.24%x12)).

The amount of ZnPc molecules non-covalently anchored on the surface of the nanotubes is found as 29.48% (22.64%/76.80%) and it is estimated that per 336 carbon atoms on ZnPc:SWCNT-non-co contains one ZnPc molecule according to the following calculation: (70.52%x1684.423)/(29.48%x12). In addition, losses of weight are about 11.73% for rGO, 15.06% for rGO-N3, 43.43% for ZnPc:rGO-co, 28.26% for ZnPc:rGO-non-co and 76.80% for ZnPc. Weight losses due to the functional groups on rGO are estimated to be 3.33, 28.37 and 17.19% for rGO-N3, ZnPc:rGO-co and ZnPc:rGO-non-co, respectively. It is estimated that per 102 carbon atoms contains one N_3 functional group on rGO-N_3. In the same way, it is estimated that per 240 carbon atoms on ZnPc:rGO-co contain one ZnPc molecule according to the calculation: (63.06x1684.423)/(36.94x12). Also, it also estimated that per 676 carbon atoms contain one ZnPc molecule on ZnPc:rGO-non-co according to the calculation: (82.81%x1684.423)/(17.19%x12).

3.2. Sensor properties study

Gas detection study is carried out for thin films of hybrid materials deposited by spin coating on glass substrates with interdigitated electrodes. The NH_3 sensing performance of the ZnPc functionalised carbon nanomaterials are evaluated and compared with sensor layers made of pristine SWCNT and rGO as reference samples. The resistance values of the obtained hybrids are around 28-29 kΩ for ZnPc:rGO and 22-23 kΩ for ZnPc:SWCNT, which are higher than those measured for pristine rGO and SWCNT (about 20 kΩ) layers. The measured resistance of pure ZnPc film is about 5000 MΩ, showing that the hybrid materials have intermediate conductivity between the Zn(II)Pc films and pristine carbon nanomaterials. The improved conductivity in the hybrid layers compared to pure ZnPc films is ascribed to the large conjugated π-system and electron transfer from ZnPc to SWCNTs or rGO sheets.

The change of the resistance of the films with time during Ar exposure is presented in Fig. 4 for ZnPc:rGO-co and ZnPc:SWCNT-co as examples. The drift of the resistance of all investigated films are quite small in Ar and can be neglected against the background of the increase of the resistance upon interaction with ammonia. Nevertheless, before starting measurements, the films were held for 10 min under Ar flow.

The sensor response of the films was determined after alternation of exposure and recovery periods in two different regimes. In the first case, the injection of NH_3 was carried out at the constant Ar flow rate of 300 ml/min. and the exposure time was fixed at 30 s. Such a dynamic regime rather than a static regime is used in some tests and it is especially useful for higher analyte concentrations in order to avoid the irreversible occupation of sites of the active sensor layer as it occurs when the material is exposed over long durations. In the second case, the Ar stream flowed through the test chamber until the resistance reached a steady state value, and then the valves of the chamber were closed and NH_3 gas (10-50 ppm) diluted with Ar was injected into the measurement cell. The resistance was recorded during a period of time necessary to obtain saturation value and calculate the response time of the sensor. Afterwards, the chamber was opened and was purged with Ar flow.

Fig. 5 demonstrates a typical normalized sensor response R_n ($R_n = (R - R_o)/R_o$; where R_o is the film resistance value at the beginning of an exposure/recovery cycle and R is the resistance of the film at a certain NH_3 concentration) of the studied films of SWCNT and their hybrids with ZnPc, measured in dynamic regime. Fig. 6 shows the normalized sensor response for rGO and its hybrids with ZnPc, measured in dynamic regime. Injection of NH_3 gas into the chamber for a period of 30 seconds leads to a noticeable increase of the films' resistance. The sensor response is highly reversible as in the case of SWCNT and its hybrids. It is worth mentioning that the resistance of SWCNT and rGO films continues to grow for some time once the injection of NH_3 gas into the chamber was stopped, while in the case of ZnPc:SWCNT hybrids the resistance starts to decrease immediately after stopping NH_3 injection (Fig. 5). In the case of ZnPc:rGO hybrids (Fig. 6) the resistance reaches its maximal value in some seconds and then starts to decrease. This different behavior of the resistance appears to be associated with different kinetics of adsorption of ammonia on the surface of the studied films.

An increase of the films' resistance upon interaction with electron donor NH_3 molecule is typical for the phthalocyanine and hybrid films possessing p-type conductivity; the electron charge transfer from NH_3 molecule to MPc results in a decrease of the holes density, hence causing a marked increase of the resistance [31]. Interaction of ZnPc with SWCNT leads to the large conjugated π-system of the hybrids and thus electron transfer from ZnPc to the carbon sheets. Both covalent and non-covalent interactions between ZnPc and SWCNT were confirmed by the red shift in the UV-vis spectra and the changes of the ratio of intensities of D and G bands in the Raman spectra [43]. The sensing behavior for MPc/rGO hybrids is similar to that described above for SWCNT and again typical for films possessing p-type conductivity [45].

The response and recovery behavior of the sensor layers of SWCNT, rGO and their hybrids were studied in more details using both dynamic and static regimes (Fig. 7). Fig. 7(a,b) shows the normalized sensor response of all investigated films versus NH_3 (40 ppm), measured in a dynamic regime at the constant Ar flow rate of 300 ml/min. and the NH_3 exposure time of

30 s. Fig. 7(c,d) shows the normalized sensor response of the same films versus NH_3 (40 ppm), measured in static regime, i.e. the resistance was recorded during a period of time necessary to obtain saturation value.

Comparison of the time dependence normalized sensor responses of rGO- and SWCNT-based films measured in static regimes (Fig. 7(c,d)) shows that the time necessary to reach saturation of the resistance is noticeably higher in the case of SWCNT and their hybrids. The response time for ZnPc:rGO-non-co, ZnPc:rGO-co and rGO films is 25, 40 and 60 s., respectively, while in the case of ZnPc:SWCNT-non-co, ZnPc:SWCNT-co and SWCNT films these values increase to 165, 220 and 305 s, respectively. The recovery time of rGO-based films is also much lower than in the case of SWCNT and ZnPc:SWCNT hybrids.

The response and recovery time of pristine SWCNTs is nearly 1.5 times as large as that of its hybrids. The recovery time of pristine rGO is also higher than that found for its hybrids; it decreases from 140 s to 90 s for both hybrids. This can be explained by faster desorption of NH_3 molecules from the surface of SWCNT shielded by phthalocyanine molecules where the latter usually having a shorter recovery time than nanocarbon materials [25, 26].

The responses of pristine SWCNT and ZnPc:SWCNT hybrid films towards NH_3, measured in dynamic regime at different concentrations are depicted in Fig. 8(a), while those of rGO and ZnPc:rGO are shown in Fig. 8(b). In the case of SWCNT-based films, the response values of ZnPc:SWCNT-co towards ammonia is higher than that of ZnPc:SWCNT-non-co, which is in good correlation with the number of ZnPc molecules adsorbed onto the SWCNT walls, as estimated by TGA (Fig. 3). The amount of ZnPc molecules covalently bonded to SWCNT is 1.8 times higher than that of ZnPc molecules non-covalently bonded to SWCNT. The correlation between the amount of adsorbed pyrene-substituted phthalocyanine molecules (MPc-py, M=Cu, Co, 2H) in SWCNT-based hybrids and their sensor responses have already been described in the literature [41]. Both SWCNT-based hybrids exhibit higher response toward NH_3

in comparison with pristine SWCNTs. These results agree with the previous data on study of the sensor responses of CNT hybrids with different MPc derivatives [40].

In contrast to SWCNT-based hybrid materials, the hybrids of rGO with the same ZnPc demonstrate lower sensor response toward NH_3 than non-functionalised rGO (Figs. 7, 8(b)), although the response of ZnPc:rGO-co is higher than that of ZnPc:rGO-non-co, correlating with the amount of ZnPc bonded with rGO according to TGA data (Fig. 3), as in the case of ZnPc:SWCNT hybrids.

Comparing the sensor response values of SWCNT- and rGO-based hybrid materials, measured in dynamic regime, we can conclude that the response of ZnPc:SWCNT-non-co and ZnPc:SWCNT-co hybrids are 5 and 9 times larger than those of the corresponding to rGO-based hybrids. According to the TGA data (Fig. 3), the amount of ZnPc molecules anchored on the surface of SWCNTs *ca* 2 times larger than on the surface of rGO.

The higher sensitivity of rGO to ammonia in comparison with its hybrids appears to be explained by the presence of residual oxygen functional groups in rGO, although it is necessary to mention that rGO properties can be dramatically based on the preparation method [46-48]. Note that the ratio of C:O in rGO used in this work was 4.77. The most characteristic features in the IR spectrum of the investigated pristine rGO are the absorption bands at 1726 cm^{-1}, which correspond to the C=O stretching vibrations of the carbonyl and carboxyl groups; the C=C vibrations at 1582 cm^{-1}, which are attributable to the sp^2 domains; the C−O epoxide stretching vibration at 1230 cm^{-1}; and the C−O vibration from the furan-like ether and hydroxyl groups at 1063 cm^{-1}. Therefore, the sensing mechanism can involve physical sorption as well as chemisorption of NH_3 mainly through hydrogen bonding at the defect sites and with the functional groups (carboxyl, carbonyl, epoxy, and hydroxyl) [46]. Functionalization of rGO with ZnPc molecule appears to cause a reduction of these active cites thus decreasing the sensor response of the rGO-ZnPc hybrids toward ammonia compared to pristine rGO. At the same time, the response of ZnPc:rGO-co hybrid is higher than that of ZnPc:rGO-non-co because the amount

of ZnPc molecules anchored on the surface of rGO in the case of covalent functionalization is *ca* 2.8 times larger than in the case of non-covalent functionalization.

The selectivity of the film was studied by measuring the change in resistance of the sensing layers in the presence of some gases and VOCs. In this regard, the films were exposed to ammonia (50 ppm), carbon dioxide (500 ppm), ethanol (700 ppm), toluene (500 ppm), dichlorobenzene (7000 ppm) and chloroform (2000 ppm) at room temperature. A comparative plot of the responses given by the sensor layers to ammonia, carbon dioxide and volatile organic compounds is shown in Fig. 9. It was found that all investigated films show higher sensitivity to ammonia compared to the other investigated analytes. It is worth pointing out that selectivity of ZnPc:SWCNT hybrids improved compared to that of pristine SWCNT.

Conclusions

In this work, ammonia gas sensing devices based on SWCNT and rGO covalently and non-covalently functionalized with 1-[N-(2-ethoxyethyl)-4-pentynamide]-8(11),15(18),22(25)-tris-{2-[2-(2-ethoxyethoxy)ethoxy]-1-[2-((2-ethoxyethoxy)-ethoxy)methyl]ethyloxy}zinc(II) phthalocyanine have been successfully fabricated and studied for the first time. The effect of covalent and non-covalent linking of the phthalocyanine both to SWCNT and to rGO on the electrical sensor response toward low concentrations of ammonia (10-50 ppm) is demonstrated. It was shown that in the case of SWCNT-based materials both covalent and non-covalent functionalisation with ZnPc leads to the increase of the sensor response toward NH_3, while functionalisation of rGO causes a decrease in the response. At the same time, both covalent and non-covalent linking of ZnPc leads to two fold decrease of the sensor recovery times. The sensor response of the SWCNT and rGO hybrids covalently functionalised with ZnPc is larger than in the case of non-covalent linking of ZnPc to carbon nanomaterials, which is in good correlation with the number of ZnPc molecules adsorbed onto the SWCNT and rGO walls, as confirmed by TG measurements.

Acknowledgments

This research did not receive any specific grant from funding agencies in the public, commercial, or not-for-profit sectors.

References

[1] A.K. Geim, K.S. Novoselov, The rise of graphene, Nat. Mater. 6 (2007) 183–191.

[2] W. Li, X. Geng, Y. Guo, J. Rong, Y. Gong, L. Wu, X. Zhang, P. Li, J. Xu, G. Cheng, M. Sun, L. Liu, Reduced graphene oxide electrically contacted graphene sensor for highly sensitive nitric oxide detection, ACS Nano. 5 (2011) 6955–6961.

[3] J.D. Fowler, M.J. Allen, V.C. Tung, Y. Yang, R.B. Kaner, B.H. Weiller, Practical chemical sensor from chemically derived graphene, ACS Nano. 3 (2009) 301–306.

[4] V. Dua, S.P. Surwade, S. Ammu, S.R. Agnihotra, S. Jain, K.E. Roberts, S. Park, R.S. Ruoff, S.K. Manohar, All-organic vapor sensor using inkjet-printed reduced graphene oxide, Angew. Chem. Int. Ed. 49 (2010) 1–5.

[5] Y. Wang, L. Zhang, N.Hu, Y. Wang, Y. Zhang, Z. Zhou, Y. Liu, S. Shen, C. Peng, Ammonia gas sensors based on chemically reduced graphene oxide sheets self-assembled on Au electrodes, Nanoscale Res. Lett. 9 (2014) 251-262.

[6] B.H. Chu, C.F. Lo, J. Nicolosi, C.Y. Chang, V. Chen, W. Strupinski, S.J. Pearton, F. Ren, Hydrogen detection using platinum coated graphene grown on SiC, Sens. Actuators B. 157 (2011) 500−503.

[7] A. Lipatov, A. Varezhnikov, P. Wilson, V. Sysoev, A. Kolmakov. A. Sinitskii, Highly selective gas sensor arrays based on thermally reduced graphene oxide, Nanoscale. 5 (2013) 5426–5434.

[8] S. Basu, P. Bhattacharyya, Recent developments on graphene and graphene oxide based solid state gas sensors, Sens. Actuators B. 173 (2012) 1–21.

[9] F. Yavari, N. Koratkar, Graphene-based chemical sensors, J. Phys. Chem. Lett. 3 (2012) 1746–1753.

[10] M. Lucci, A. Reale, A. Di Carlo, S. Orlanducci, E. Tamburri, M.L. Terranova, I. Davoli, C. Di Natale, A. D'Amico, R. Paolesse, Optimization of a NOx gas sensor based on single walled carbon nanotubes, Sens. Actuators B. 118 (2006) 226–231.

[11] D. R. Kauffman, A. Star, Single-walled carbon-nanotube spectroscopic and electronic field-effect transistor measurements: a combined approach, Small. 3 (2007) 1324-1329.

[12] A. Kleinhammes, S.H. Mao, X.J. Yang, X.P. Tang, H. Shimoda, J.P. Lu, O. Zhou, Y. Wu, Gas adsorption in single-walled carbon nanotubes studied by NMR, Phys. Rev. B. 68 (2003) 075418.

[13] E. Liu, X. Zhang, Electrochemical sensor for endocrine disruptor bisphenol a based on a glassy carbon electrode modified with silica and nanocomposite prepared from reduced graphene oxide and gold nanoparticles, Anal. Meth. 6 (2014) 8604–8612.

[14] D.Y. Fu, G.Y. Han, Y.Z. Chang, J.H. Dong, The synthesis and properties of ZnO graphene nanohybrid for photodegradation of organic pollutant in water, Mater. Chem. Phys. 132 (2012) 673-681.

[15] K. Zhang, K.C. Kemp, V. Chandra, Homogeneous anchoring of TiO2 nanoparticles on graphene sheets for waste water treatment, Mater. Lett. 81 (2012) 127-130.

[16] T.-Y. Huang, C.-W. Kung, H.-Y. Wei, K.M. Boopathi, C.-W. Chu, K.-C. Ho, A high performance electrochemical sensor for acetaminophen based on a rGO–PEDOT nanotube composite modified electrode, J. Mater. Chem. A 2 (2014) 7229–7237.

[17] Y. Zhou, Y.Jiang, G. Xie, M. Wu, H. Tai, Gas sensors for CO2 detection based on RGO–PEI films at room temperature, Chin. Sci. Bull. 59 (2014) 1999–2005.

[18] Y. Xiao, Q. Yang, Z. Wang, R. Zhang, Y. Gao, P. Sun, Y. Sun, G. Lu, Improvement of NO2 gas sensing performance based on discoid tinoxide modified by reduced graphene oxide, Sens. Actuators B. 227 (2016) 419–426.

[19] S. Liu, B. Yu, H. Zhang, T. Fei, T. Zhang, Enhancing NO2 gas sensing performances at room temperature based on reduced graphene oxide-ZnO nanoparticles hybrids, Sens. Actuators B. 202 (2014) 272–278.

[20] D. Zhang, H. Chang, P. Li, R. Liu, Characterization of nickel oxide decorated-reduced graphene oxide nanocomposite and its sensing properties toward methane gas detection, J. Mater. Sci. Mater. Electron. 27 (2016) 3723–3730.

[21] D. Guo, P. Cai, J. Sun, W. He, X. Wu, T. Zhang, X. Wang, X. Zhang, Reduced-graphene-oxide/metal-oxide p-n heterojunction aerogels as efficient 3D sensing frameworks for phenol detection, Carbon. 99 (2016) 571-578.

[22] V. Srivastava, K. Jain, At room temperature graphene/SnO2 is better than MWCNT/SnO2 as NO2 gas sensor, Mater. Lett. 169 (2016) 28–32.

[23] J.T. Robinson, F.K. Perkins, E.S. Snow, Z. Wei, P. E. Sheehan, Reduced graphene oxide molecular sensors, Nano Lett. 8 (2008) 3137-3140.

[24] X.Q. Zhang, Y.Y. Feng, S.D. Tang, W. Feng, Preparation of a graphene oxide-phthalocyanine hybrid through strong π-π interactions, Carbon. 48 (2010) 211–216.

[25] X. Zhou, X. Wang, B. Wang, Z. Chen, C. He, Y. Wu, Preparation, characterization and NH3-sensing properties of reduced graphene oxide/copper phthalocyanine hybrid material, Sens. Actuators B. 193 (2014) 340–348.

[26] H.S. Dehsari, J.N. Gavgani, A. Hasani,M. Mahyari, E.K. Shalamzari, A. Salehi, F.A. Taromi, Copper (II) phthalocyanine supported on a three dimensional nitrogen-doped graphene/PEDOT-PSS nanocomposite as a highly selective and sensitive sensor for ammonia detection at room temperature, RSC Adv. 5 (2015) 79729–79737.

[27] G. Bottari, J.A. Suanzes, O. Trukhina, T. Torres, Phthalocyanine-carbon nanostructure materials assembled through supramolecular interactions, J. Phys. Chem. Lett. 2 (2011) 905–913.

[28] B. Wang, Y. Wu, X. Wang, Z. Chen, C. He, Copper phthalocyanine noncovalent functionalised single-walled carbon nanotube with enhanced NH3 sensing performance, Sens. Actuators B. 190 (2014) 157-164.

[29] L. Zhao, S. Zhu, J. Zhou, A novel amperometric nitric oxide sensor based on imprinted microenvironments for controlling metal coordination, Sens. Actuators B. 171 (2012) 563-571.

[30] I. Kim, H. Li, Fabrication and applications of carbon nanotube-based hybrid nanomaterials by means of non-covalently functionalised carbon nanotubes, in: Nanotechnology and Nanomaterials. Carbon Nanotubes - From Research to Applications, S. Bianco (Ed.), INTECH chapter 13, 2011.

[31] X. Li, B. Wang, X. Wang, X. Zhou, Z. Chen, C. He, Z. Yu, Y. Wu, Enhanced NH3-sensitivity of reduced graphene oxide modified by tetra-α-iso-pentyloxymetallophthalocyanine derivatives, Nanoscale Res. Lett. 10 (2015) 373-385.

[32] H. Hosseini, M. Mahyari, A. Bagheri, A. Shaabani, A novel bioelectrochemical sensing platform based on covalently attachment of cobalt phthalocyanine to graphene oxide, Biosens. Bioelectron. 52 (2014) 136–142.

[33] N. Karousis, J. Ortiz, K. Ohkubo, T. Hasobe, S. Fukuzumi, A. Sastre-Santos, N. Tagmatarchis, Zinc phthalocyanine-graphene hybrid material for energy conversion: Synthesis, characterization, photophysics, and photoelectrochemical cell preparation, J. Phys. Chem. C. 116 (2012) 20564−20573.

[34] A.L. Verma, S. Saxena, G.S.S. Saini, V. Gaur, V.K. Jain, Hydrogen peroxide vapor sensor using metal-phthalocyanine functionalised carbon nanotubes, Thin Solid Films. 519 (2011) 8144–8148.

[35] P. Jha, M. Sharma, A. Chouksey, P. Chaturvedi, D. Kumar, G. Upadhyaya, J.S.B.S Rawat, P.K. Chaudhury, Functionalisation of carbon nanotubes with metal phthalocyanine for selective gas sensing application, Synth. React. Inorg. Metal-Org. Nano-Metal Chem. 44 (2014) 1551–1557.

[36] T. Mugadza, T. Nyokong, Electrochemical, microscopic and spectroscopic characterization of benzene diamine functionalised single walled carbon nanotube-cobalt (II) tetracarboxy-phthalocyanine conjugates, J. Coll. Interface Sci. 354 (2011) 437–447.

[37] Y. Wang, N. Hu, Z. Zhou, D. Xu, Z. Wang, Z. Yang, H. Wei, E.S.-W. Kong, Y. Zhang, Single-walled carbon nanotube/cobalt phthalocyanine derivative hybrid material: Preparation, characterization and its gas sensing properties, J. Mater. Chem. 21 (2011) 3779–3787.

[38] K. H. Le Ho, L. Rivier, B. Jousselme, P. Jergou, A. Filoramoa, S. Campidelli, Zn-porphyrin/Zn-phthalocyanine dendron for SWNT functionalisation, Chem. Commun. 46 (2010) 8731–8733.

[39] H. Banimuslem, A. Hassan, T. Basova, A. A. Esenpınar, S. Tuncel, M. Durmuş, A.G. Gürek, V. Ahsen, Dye-modified carbon nanotubes for the optical detection of amines vapours, Sens. Actuators B. 207 (2015) 224–234.

[40] E.N. Kaya, S. Tuncel, T.V. Basova, H. Banimuslem, A. Hassan, A.G. Gürek, V. Ahsen, M. Durmuş, Effect of pyrene substitution on the formation and sensor properties of phthalocyanine-single walled carbon nanotube hybrids, Sen. Actuators B. 199 (2014) 277–283.

[41] E.N. Kaya, T. Basova, M. Polyakov, M. Durmuş, B. Kadem, A. Hassan, Hybrid materials of pyrene substituted phthalocyanines with single-walled carbon nanotubes: structure and sensing properties, RSC Adv. 5 (2015) 91855–91862.

[42] S. Tuncel, E. N. Kaya, M. Durmuş, T. Basova, A. G. Gürek, V. Ahsen, H. Banimuslem, A. Hassan, Distribution of single-walled carbon nanotubes in pyrene containing liquid crystalline asymmetric zinc phthalocyanine matrix, Dalton Trans. 43 (2014) 4689–4699.

[43] B. Kadem, M. Göksel, A. Şenocak, E. Demirbaş, D. Atilla, M. Durmuş, T. Basova, K. Shanmugasundaram, A. Hassan, Effect of covalent and non-covalent linking on the structure, optical and electrical properties of novel zinc(II) phthalocyanine functionalised carbon nanomaterials, Polyhedron. 110 (2016) 37–45.

[44] R.M.A. Azzam, The intertwined history of polarimetry and ellipsometry, Thin Solid Films 519 (2011) 2584-2588.

[45] S.S. Varghese, S.H. Varghese, S. Swaminathan, K. K. Singh, V. Mittal, Two-dimensional materials for sensing: Graphene and beyond, Electronics 4 (2015) 651-687.

[46] E.C. Mattson, K. Pande, M. Unger, S. Cui, G. Lu, M. Gajdardziska-Josifovska, M. Weinert, J. Chen, C.J. Hirschmug, Exploring adsorption and reactivity of NH3 on reduced graphene oxide, J. Phys. Chem. C. 117 (2013) 10698−10707.

[47] S. Mao, H.H. Pu, J.H. Chen, Graphene oxide and its reduction: Modeling and experimental progress, RSC Adv. 2 (2012) 2643−2662.

[48] R. Ghosh, A. Midya, S. Santra, S.K. Ray, P.K. Guha, Chemically reduced graphene oxide for ammonia detection at room temperature, ACS Appl. Mater. Interfaces. 5 (2013) 7599−7603.

Figure Captions

Figure 1. Scheme of ZnPc and covalently bonded ZnPc:SWCNT-co and ZnPc:rGO-co hybrid materials.

Figure 2. SEM images of thin films of ZnPc:SWCNT-non-co (a), ZnPc:SWCNT-co (b), ZnPc:rGO-non-co (c) and ZnPc:rGO-co (d) hybrids.

Figure 3. Thermogravimetric analysis of ZnPc:SWCNT-non-co, ZnPc:SWCNT-co, ZnPc:rGO-non-co, ZnPc:rGO-co in comparison with pristine SWCNT, SWCNT-N3 and ZnPc.

Figure 4. Variation of the resistance of the ZnPc:rGO-co and ZnPc:SWCNT-co films with time during Ar exposure and NH_3 (40 ppm) injection.

Figure 5. Normalized sensor response of thin films of pristine SWCNT, ZnPc:SWCNT-co and ZnPc:SWCNT-non-co hybrids vs NH_3 (10-50 ppm), measured in a dynamic regime at the constant Ar flow rate of 300 ml/min. and the exposure time of 30 s.

Figure 6. Normalized sensor response of thin films of rGO, ZnPc:rGO-co and ZnPc:rGO-non-co hybrids vs NH_3 (10-50 ppm), measured in a dynamic regime at the constant Ar flow rate of 300 ml/min. and the exposure time of 30 s.

Figure 7. Normalized sensor response of thin films of SWCNT, ZnPc:SWCNT-co, ZnPc:SWCNT-non-co hybrids, rGO, ZnPc:rGO-co and ZnPc:rGO-non-co hybrids vs NH_3 (40 ppm), measured in a dynamic regime at the constant Ar flow rate of 300 ml/min. and the exposure time of 30 s (a, b) and static regime (c, d).

Figure 8. Responses of pristine SWCNT and ZnPc:SWCNT hybrid films (a), rGO and ZnPc:rGO hybrid films (b) vs NH_3 concentrations.

Figure 9. Response of SWCNT, rGO and their hybrids to ammonia (50 ppm), carbon dioxide (500 ppm), ethanol (700 ppm), toluene (500 ppm), dichlorobenzene (7000 ppm) and chloroform (2000 ppm).

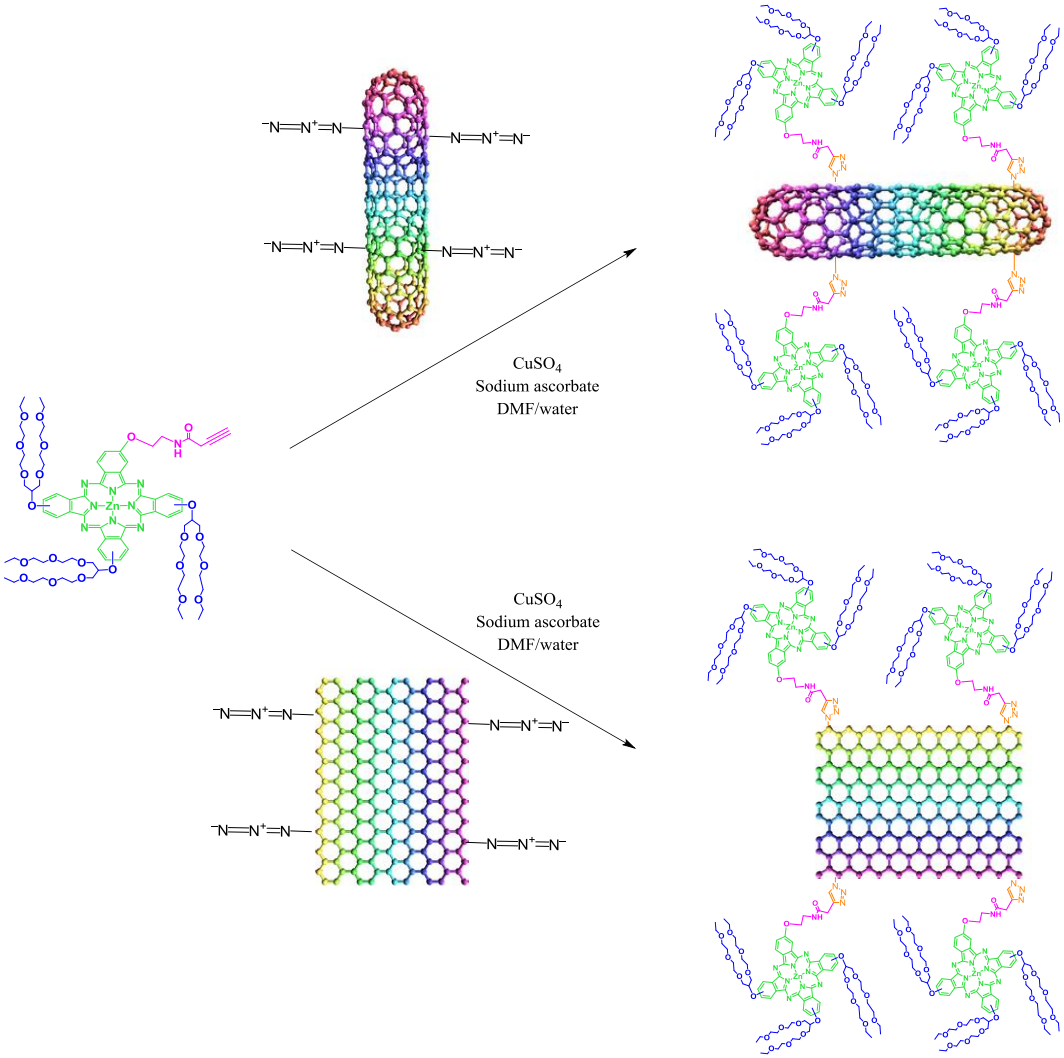

Figure 1. Scheme of ZnPc and covalently bonded ZnPc:SWCNT-co and ZnPc:rGO-co hybrid materials.

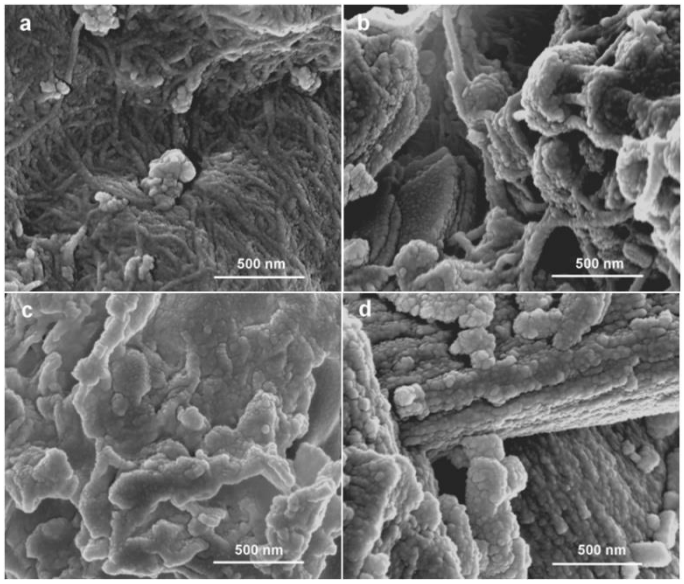

Figure 2. SEM images of the films of ZnPc:SWCNT-non-co (a), ZnPc:SWCNT-co (b), ZnPc:rGO-non-co (c) and ZnPc:rGO-co (d) hybrids.

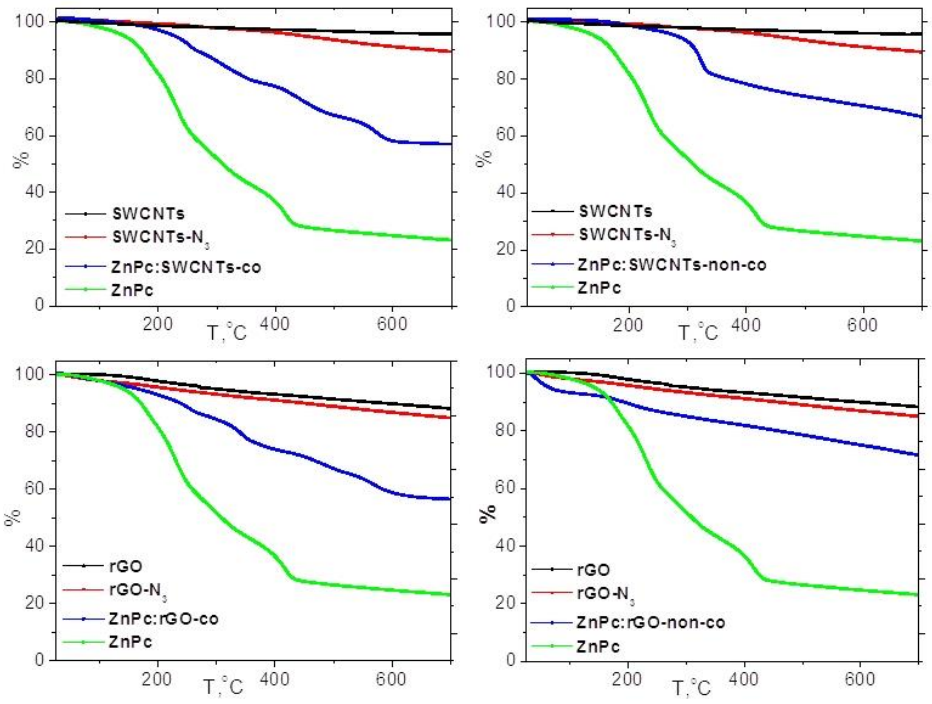

Figure 3. Thermogravimetric analysis of ZnPc:SWCNT-non-co, ZnPc:SWCNT-co, ZnPc:rGO-non-co, ZnPc:rGO-co in comparison with pristine SWCNT, SWCNT-N_3 and ZnPc.

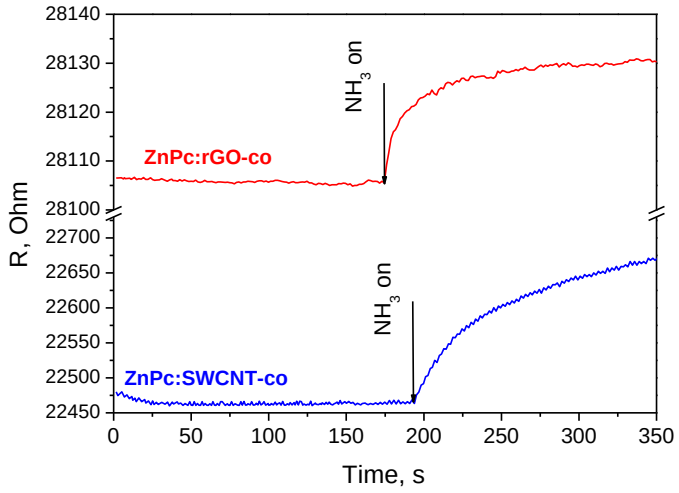

Figure 4. Variation of the resistance of the ZnPc:rGO-co and ZnPc:SWCNT-co films with time during Ar exposure and NH_3 (40 ppm) injection.

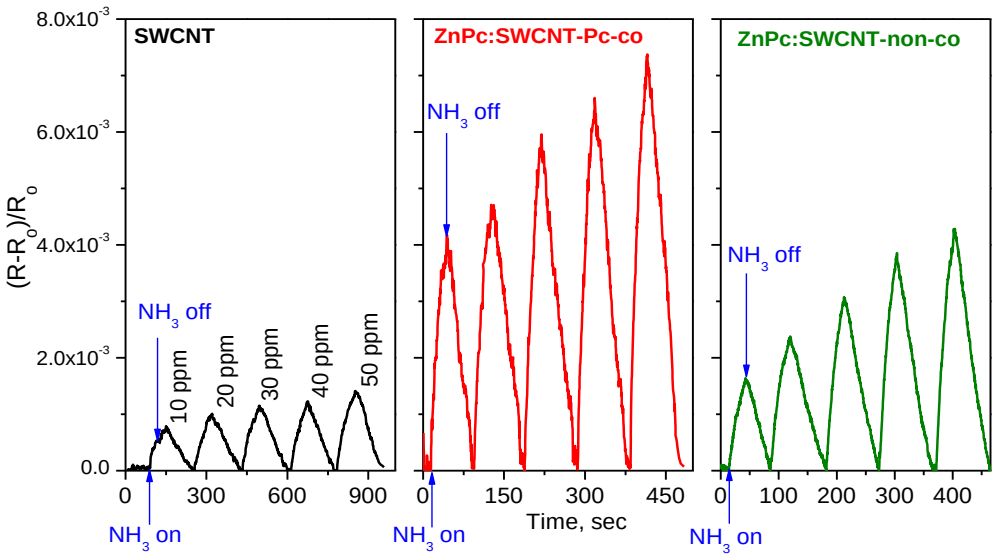

Figure 5. Normalized sensor response of thin films of pristine SWCNT, ZnPc:SWCNT-co and ZnPc:SWCNT-non-co hybrids vs NH_3 (10-50 ppm), measured in a dynamic regime at the constant Ar flow rate of 300 ml/min. and the exposure time of 30 s.

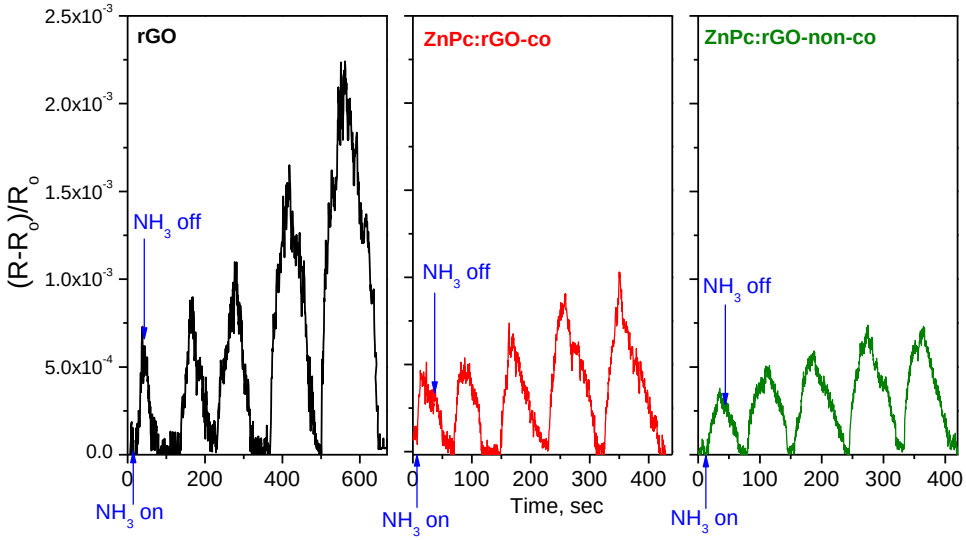

Figure 6. Normalized sensor response of thin films of rGO, ZnPc:rGO-co and ZnPc:rGO-non-co hybrids vs NH_3 (10-50 ppm), measured in a dynamic regime at the constant Ar flow rate of 300 ml/min. and the exposure time of 30 s.

.

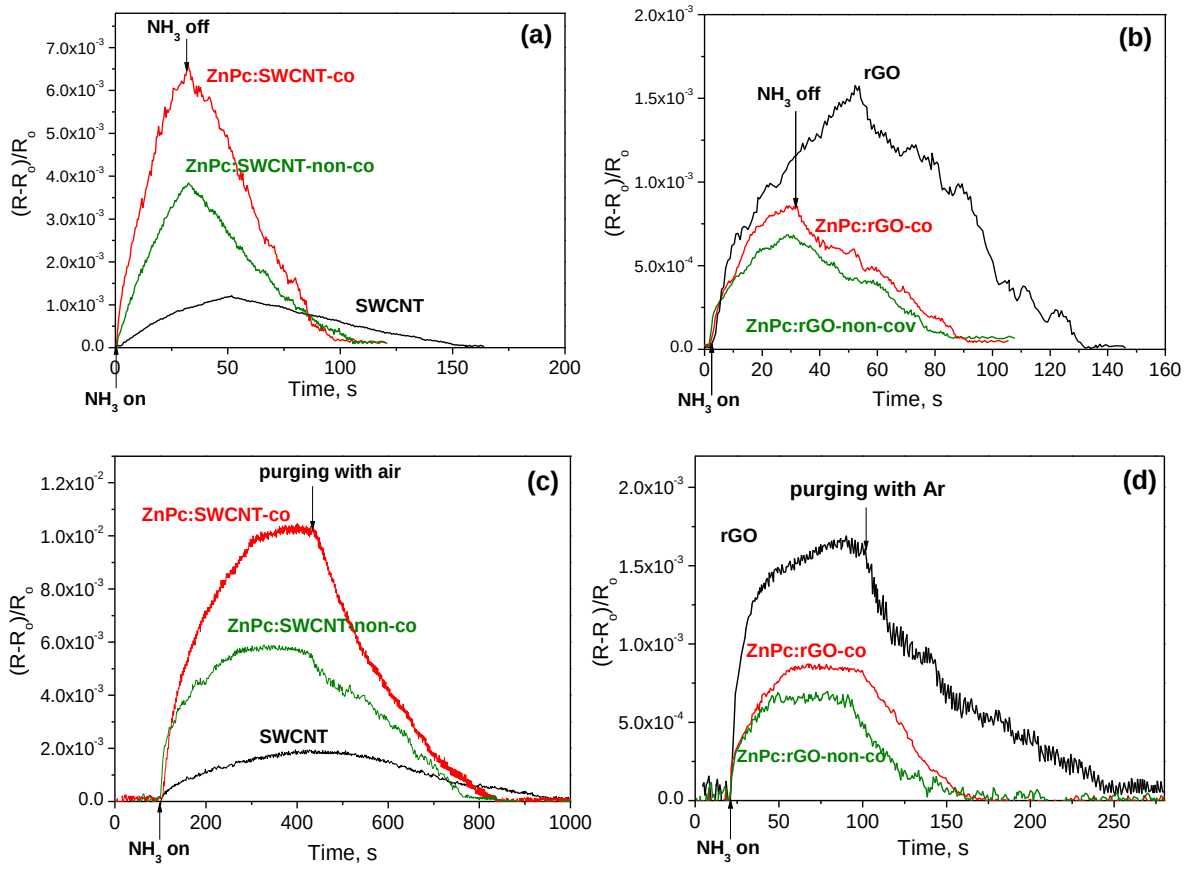

Figure 7. Normalized sensor response of thin films of SWCNT, ZnPc:SWCNT-co, ZnPc:SWCNT-non-co hybrids, rGO, ZnPc:rGO-co and ZnPc:rGO-non-co hybrids vs NH_3 (40 ppm), measured in a dynamic regime at the constant Ar flow rate of 300 ml/min. and the exposure time of 30 s (a, b) and static regime (c, d).

.

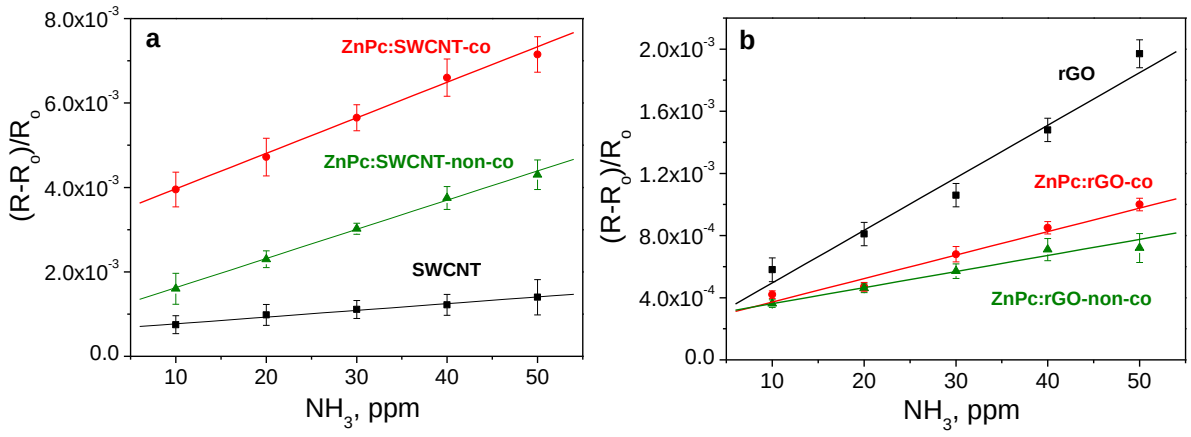

Figure 8. Responses of pristine SWCNT and ZnPc:SWCNT hybrid films (a), rGO and ZnPc:rGO hybrid films (b) vs NH_3 concentrations.

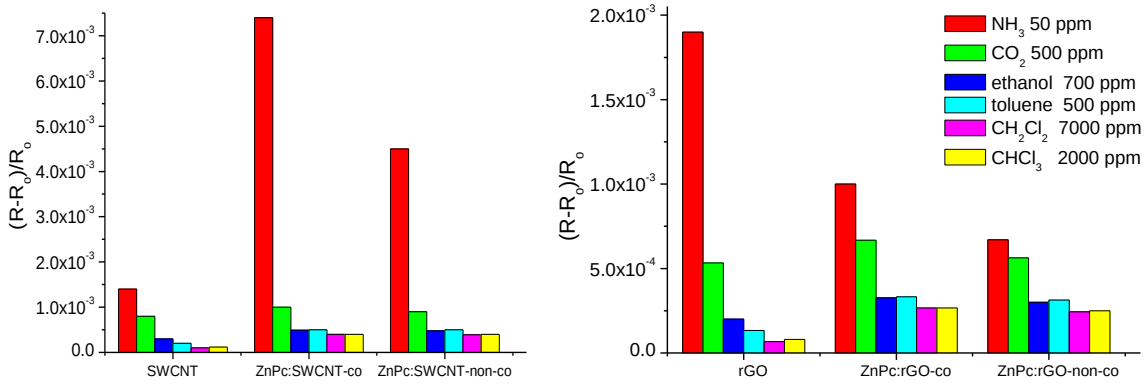

Figure 9. Response of SWCNT, rGO and their hybrids to ammonia (50 ppm), carbon dioxide (500 ppm), ethanol (700 ppm), toluene (500 ppm), dichlorobenzene (7000 ppm) and chloroform (2000 ppm).